Automatic Precipitation Measurement Based on Raindrop Imaging and Artificial Intelligence

Chi-Wen Hsieh, *Member*, *IEEE*, Po-Wei Chi, Chih-Yen Chen, *Senior Member*, *IEEE*, Chun-Jen Weng, *Member*, *IEEE*, and Lijuan Wang, *Member*, *IEEE*

***Abstract*—Rainfall measurement is subject to various uncertainties owing to the complexity of measurement techniques and atmosphere characteristics associated with weather type. Thus, this study presents a video-based disdrometer to analyze raindrop images by introducing artificial intelligence technology for the rainfall rate. First, a high-speed CMOS camera is integrated into a planar LED as a backlight source for appropriately acquiring falling raindrops in different positions. The falling raindrops can be illuminated and used for further image analysis. Algorithms developed for raindrop detection and trajectory identification are employed. In a field test, a rainfall event of 42 continuous hours has been measured by the proposed disdrometer that is validated against a commercial PARSIVEL^2 disdrometer and a tipping-bucket rain gauge at the same area. In the evaluation for 5-min rainfall images, the results of the trajectory identification are within the precision of 87.8%, recall of 98.4%, and F1 score of 92.8%, respectively. Furthermore, the performance exhibits that the rainfall rate and raindrop size distribution obtained by the proposed disdrometer is remarkably consistent with those of PARSIVEL^2 disdrometer. The performance suggests that the proposed disdrometer based on the continuous movements of the falling raindrops can achieve accurate measurements and eliminate the potential errors effectively in the real-time monitoring of rainfall.**

***Index Terms*—Rainfall rate, Raindrop size distribution, Disdrometer, In situ atmospheric observations, Particle tracking velocimetry (PTV)**

I. Introduction

Owing to the effect of climate change, precipitation monitoring is applied to provide useful applications, such as meteorology, hydrology and agriculture [1]. Rainfall measurement nowadays attracts wide attention and has a critical role in socioeconomic activities. Because the observation of rainfall rate is extremely heuristic and complex, many precipitation measurement technologies have been developed. In the past, precipitation over a large area was typically measured by weather radar and satellite, i.e. the assessment of the Z-R relationship between radar reflectivity (Z) and rainfall rate (R) with the assumption of time- and space- invariance [2-5]. To eliminate the deviations of remote sensing data, characteristics of raindrop spectra are critical in the calibration procedure.

Direct observation of cloud droplets is the best method to study precipitation behaviors; however, the entire process is either time-consuming or costly. [6, 7]. From another viewpoint, raindrop observation on the ground is relatively simple owing to many advanced disdrometers [8]. The measurement of the raindrop size distribution (RSD) by such instruments can provide essential information for tracing precipitation processes, accounting for rainfall, and understanding microphysics in numerical weather models [9]. Hitherto, an optical type of disdrometer is becoming the most popular instrument for rainfall observations. Löffler-Mang et al. reported the particle size velocity (PARSIVEL) disdrometer, which is a commercial disdrometer for monitoring precipitation, hail, and snow [10]. Additionally, the same concept is extended to a two-dimensional video disdrometer (2DVD) to observe more complete three-dimensional information about a raindrop [11]. Unfortunately, they suffer from different degrees of raindrop mismatches during sensing [12,13]. In the recent decade, Saylor et al. adopted different edge detection algorithms for various depths to acquire more accurate raindrop images [14]. However, measurements by this approach performed outdoors remains uncertainty. Later, Testik et al. has reported a high-speed optical disdrometer for measuring rainfall microphysical quantities [13]. The issue is that only raindrops around the focal plane of a camera can be counted for further analysis, and little work has been considered regarding its practical efficacy. With recent developments in technology and image processing tools, object detection and particle image velocimetry/particle tracking velocimetry (PIV/PTV) have been extensively applied in many fields. PIV/PTV technologies are based on the visualization analysis of flow with high spatial and temporal resolutions to overcome the difficulties of direct tracking [15]. To the best of our knowledge, few attempts have been reported regarding raindrop characterization and the rainfall rate estimation based on this method [16, 17]. This could be owing to the wide range sizes and corresponding velocity distributions of falling raindrops that render the tasks

This work was supported by the Ministry of Science and Technology of Taiwan R.O.C. (MOST 107-2221-E-492-027).

C. W. Hsieh and P. W. Chi are with the Department of Electrical Engineering, National Chiayi University, Chiayi City 60004 (e-mail: chiwen@mail.ncyu.edu.tw; kevin61605@gmail.com).

C. Y. Chen and C. J. Weng are with Instrument Technology Research Center, National Applied Research Laboratories, Hsinchu 30076, Taiwan (e-mail: chihyenorama@gmail.com; cjweng@itrc.narl.org.tw).

Lijuan Wang is in electronic instrumentation with the School of Engineering and Digital Arts, University of Kent, CT2 7NT, U.K. (e-mail: l.wang@kent.ac.uk).

challenging. In some cases, wind-caused turbulences can impose a bias on the two parameters and affect the measurement. Likewise, the detection and tracking of many nonrigid bodies cannot sufficiently provide features to facilitate computations using PIV/PTV technologies [17-19]. Finally, the direct use of backlight illumination restricts the observation because of the out-of-focus images, e.g., only the raindrops in the narrow depth of the field can be recognized correctly in the study.

Recently, many reports have indicated the significant progress of artificial neural network (ANN) methodologies in PIV/PTV technologies; thus, it can be explored to solve some of the limitations of the current approaches [20-23]. The architecture of an ANN can be regarded as a nonlinear process. Among them, the back-propagation network (BPN) is the most typical model that relates the inputs and outputs of a complex function. Furthermore, their interconnections are formed by turning the weights and biases iteratively to minimize the squared error sum between the actual output of the BPN and the desired output through a supervised learning algorithm. The minimization process is typically performed by adopting the gradient- or steepest- descent methods [24]. Consequently, ANNs can extract key features to classify or predict tasks and provide an efficient computation with adaptability and robustness.

Despite the numerous reports regarding the ANN's capability in performing computations in the current PIV/PTV technologies, some existing limitations must be addressed [23,25-27]. To investigate into the measurement of raindrops, efficient and reliable PIV/PTV technologies are necessary. The trajectory and shape of a raindrop may be useful features, and a tailored ANN model is expected to incorporate them to yield a better performance than the tasks using the current algorithms [28, 29]. One can therefore expect that a well-designed ANN technology is conducted to improve analytical models. This new technique is applicable to raindrop measurement, thus avoiding ambiguous particle pairings and trajectory deviations.

The purpose of this study is to achieve ground rainfall measurement. A video-based disdrometer is proposed by integrating a low-cost CMOS camera for a high-speed image acquisition, a planar LED as a backlight source, and a specific lens for increasing the depth. Falling raindrops can be illuminated and the raindrop images are captured for the analysis. In particular, we have applied ANN classification for six extracted features from the detected raindrops to perform the trajectory identification algorithm. Thus, the rainfall rate, accumulated rainfall rate, and RSD can be estimated. Subsequent sections contain descriptions that are more complete about the proposed disdrometer and its performance in an outdoor field experiment. The final section presents our conclusions about the primary contributions and some empirical findings for the characterization of raindrops.

II. Rainfall Measurement System

The proposed video-based disdrometer attempts to analyze falling raindrops and the corresponding raindrop properties. The system design and workflow are described as follows:

A. System design and primary components

The optomechanic system of the video-based disdrometer includes three primary components: a light source, camera, and system controller. The layout is illustrated in Fig. 1. The left component is a planar LED light source with a diffuser to generate a flat and uniform illumination. The center wavelength of the LED light is within 460 nm instead of longer wavelengths or broad band light sources; thus, the edges of the raindrops can be highlighted to facilitate detection.

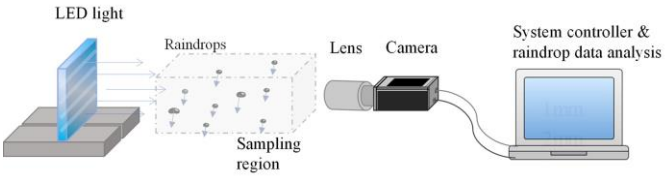

Fig. 1. Schematic layout of the video-based disdrometer for measuring rainfall rate.

According to the available evidence in previous studies, the sizes of the primary raindrops range substantially from 0.5 mm to 5 mm, thus indicating that the falling speed of a raindrop ranges from 2 to almost 10 m/s [30, 31]. This implies that spatial resolution is required to resolve the minimum small-scale of 0.5 mm. Moreover, the fast shutter speed (i.e. short exposure time) of the camera should enable the raindrop images to be captured instantaneously. Unfortunately, the cost of a high-speed camera and the vast amount of raindrop imaging data hamper the development of such technique. Owing to the availability of a high-speed CMOS camera and limit budget, the functionality of fast image acquisition can be implemented. The CMOS camera was setting at 500-Hz frame rate, 69-μs exposure time, and 82-μm resolution. To prevent optical distortions of the raindrop images within different depths, an optical lens is mounted to provide a depth of 120 mm to ensure almost unchanged shapes of the raindrops. Therefore, the imaging system is can produce a field of view of 52.5 mm × 39.0 mm. The configurations of the system are listed in Table I.

TABLE I
System Configurations

Item	Value	Description
FOV	52.5 mm ×39.0 mm	Physical imaging area of the system
CMOS size	3.1 mm × 2.3 mm	Practical camera chip size
Depth of field	120 mm	Focusing depth of the lens
Resolution	82.0 μm	Pixel size of the physical area
Frame rate	500 Hz	Acquisition frames per second
Exposure time	69 μs	Time of the open shutter duration

Finally, a laptop is employed as a control unit to manage the camera with the frame capturing and perform image processing procedures. The computation module synchronizes the operation of the camera and light source according to the trigger signals received from the computer.

B. Proposed flowchart

To explain the developed algorithm of our proposed disdrometer, a workflow diagram is illustrated in Fig. 2. The workflow can be divided into two parts: rainfall monitoring and

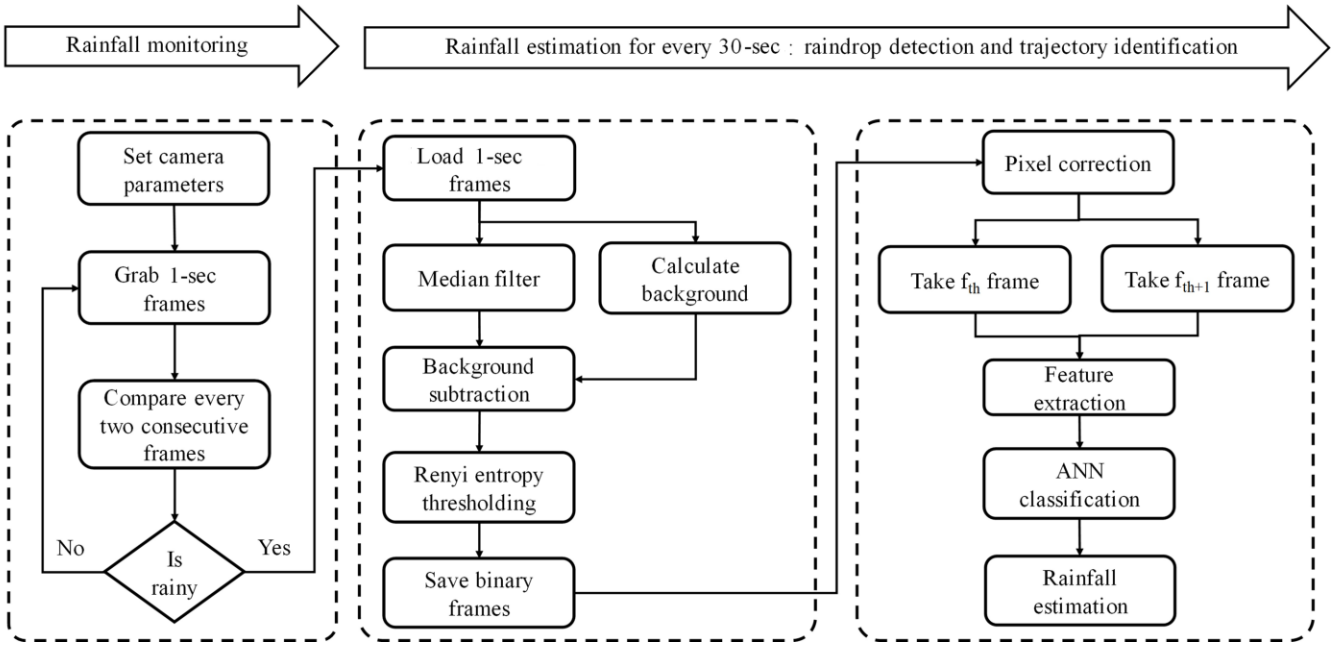

Fig. 2. Workflow diagram of the raindrop detection and trajectory identification procedures.

rainfall estimation. The first procedure is to monitor whether it is raining. The second procedure can be further subdivided into two parts consisting of raindrop detection and trajectory identification with feature extraction, and ANN classification and verification.

1) Rainfall monitoring: The proposed system sets a timer to trigger the light and a camera and process 1-sec monitoring every minute. If the suspicious raindrops are appealing in the sampling region, the rainy condition can be determined by performing raindrop evaluation between the previous and subsequent frames. Meanwhile, if the raindrops are detected continually, the rainfall monitoring status will proceed to the next stage of the rainfall estimation. This predetermined operation can reduce power consumption, computation resources and storage space requirements.

2) Rainfall estimation: Following the above, the rainfall estimation including raindrops detection and trajectory identification will be launched once every 30-sec periodically. Consequently, the rainfall parameters can be obtained to present the rainfall rate and RSD. For automation, the proposed system will continue operation until no precipitation raindrops are detected for a period by the time set.

III. Raindrop Detection and Trajectory Identification

In the experiment, because of the short exposure and susceptibility to interferences of the CMOS sensor, the acquired images are easily affected by random noises. Additionally, dust and dirt on the lens may cause unexpected consequences. The preprocessing procedures are key tasks assisting raindrop detection and the deletion of empty images that contain no raindrops. As the duration of 30-sec for each operation is sufficient, the rainfall estimation has adequate time to process the raindrop images. In the following, the framework of the raindrop detection and the trajectory identification are introduced.

A. Raindrop detection algorithm

The raindrops are identified according to the blocked light intensity in a number of consecutive frames. Thus, the image preprocessing procedures are used to correct the nonhomogeneity of the light source and eliminate artifacts. The collocation procedures are presented below:

1) Introduce a median filter with a 3×3 window for image smoothing;
2) Average the acquired 500 images for each time period to construct a background;
3) Perform a background correction for the 500 images;
4) Employ a segmentation method, i.e., the Renyi entropy [32], to separate the raindrops from the images;
5) Apply a minimum bounding box to replace a raindrop image with the horizontal and vertical displacements, canting angle, and major and minor axes.

B. Trajectory identification by ANN

To observe the frame-by-frame falling motion of the raindrops, several characteristics from the precipitation are extracted for achieving particle tracking. The detailed execution procedures are explained in Appendix A. Our algorithm that is used to link raindrops from only two frames is based on an iterative estimation. Subsequently, by analyzing the similarities of the shape, orientation, and movement as expected for each raindrop in consecutive frames, the trajectory can be identified accurately. The operative procedures are shown as follows:

1) Apply pixel correction for each detected raindrop, whose framework is shown in Appendix B;
2) Input the six extracted features, such as the horizontal and vertical displacements, area, canting angle, and major and minor axes, into the designed ANN classification;
3) Estimate all cost values of the trajectories for each raindrop in the previous frame associated with all the raindrops in the subsequent frame;
4) Employ an intersection layer to determine the best suitable trajectory frame by frame;
5) Derive the rainfall rate, accumulated rainfall rate, and RSD.

IV. Results and Discussions

Field tests in an outdoor environment were performed during a rainfall event in Hsinchu, Taiwan, which occurred from 00:00 on June 16th to 18:00 on June 17th, 2017 (UTC). After applying the filtering process for those frames without raindrops, 246280 frames underwent analysis.

A. ANN classification for rainfall evaluation

The model processes were used for evaluating the performance of the trajectory identification. The ANN classification was used for the 5-min testing data of rainfall images. The results are displayed in Fig. 3. The learning curve approaches 2×10^4 epochs. The results yield an accuracy rate of 0.962 and 0.960 for the testing data and validation data, respectively, when the learning curve achieves 1×10^4 epochs. In the evaluation, the results are derived with a precision of 87.8%, recall of 98.4% and F1 score of 92.8%, which are expressed as Eqs. (1), (2), and (3), respectively. All images of the testing data were manually labeled with the raindrop linking status.

$$Precision(\%) = \frac{True\ positive}{True\ positive + False\ positive} \quad (1)$$

$$Recall(\%) = \frac{True\ positive}{True\ positive + False\ negative} \quad (2)$$

$$F1\ score(\%) = \frac{2}{1/Precision + 1/Recall} \quad (3)$$

Subsequently, three different types of rainfall rates of 14:41(high rainfall), 15:36(medium rainfall) and 17:12(low rainfall) were selected for further observation. Table II lists the classification performance; only a few cases were misidentified as either a heavy rainfall or the medium rainfall. The result proves that the proposed algorithm of trajectory identification performs well.

TABLE II
ANN classification for rainfall evaluation at 14:41(heavy), 15:36(medium) and 17:12(low) in June 16th, 2017 by manual verification.

	Validity	Spurious	Non-matched
Heavy rainfall	186 (97.0%)	5 (3.0%)	3
Medium rainfall	87 (95.6%)	4 (4.4%)	2
Small rainfall	47 (100.0%)	0 (0.0%)	1

B. Rainfall rate measurement

To understand the differences among different measuring technologies, the proposed disdrometer and the collocated PARSIVEL^2 disdrometer are both operated for the 42-hr continuous rainfall event in the same space. In addition, a tipping-bucket rain gauge with a resolution of 1 mm and an hourly update was used as a reference standard in the measurement. Subsequently, the rainfall rate and accumulated rainfall rate were obtained. The performance is shown in Fig. 4. Our finding indicates that the annual hour-by-hour rainfall rate of the proposed system is highly correlated with the PARSIVEL^2 measurement, and only a relatively small variation is observed regardless of whether the rainfall rate is large or small. The measurement reaches average rainfall rate values at 2.50 mm/h for the proposed disdrometer, 2.62 mm/h for the

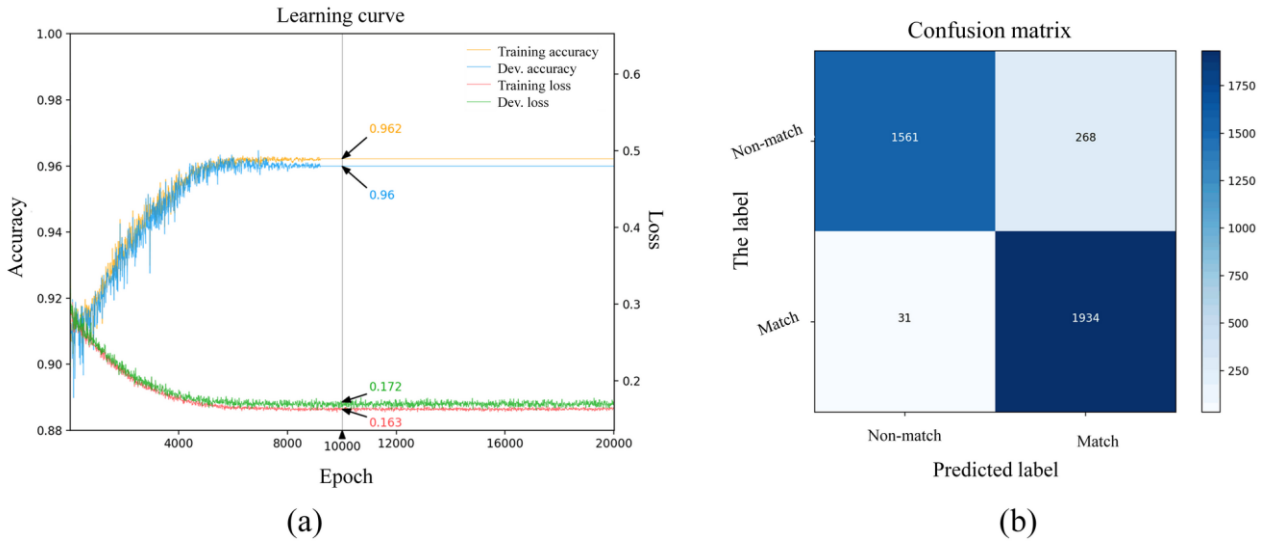

Fig. 3. Results of ANN classification for the rainfall images by (a) the learning curve and (b) the confusion matrix.

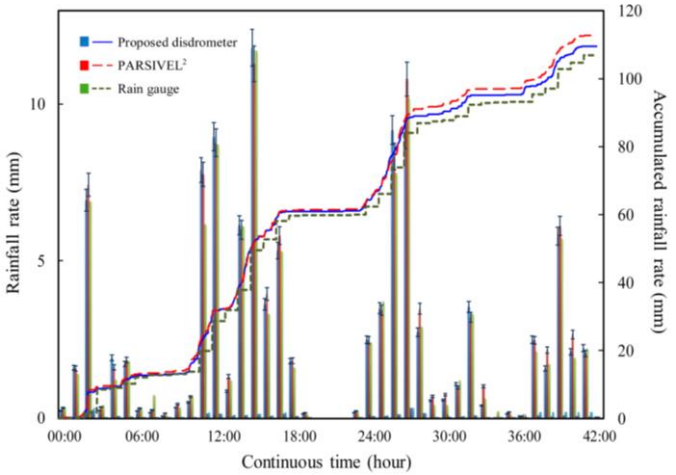

Fig. 4. Rainfall rate and accumulated rainfall rate of the proposed video-based disdrometer (blue color), PARSIVEL² disdrometer (red color) and rain gauge (green color) measured within 42 continuous hours from 00:00 on June 16th, 2017.

PARSIVEL² disdrometer and 2.45 mm/h for the rain gauge. For the observation of accumulated rainfall rate, the three approaches exhibit an increasing trend, and the accumulated rainfall rates are 109.51 mm for the proposed disdrometer, 112.71 mm for the PARSIVEL² and 106.9 mm for the rain gauge. The experimental results are in the reasonable scope.

C. RSD measurement

In the RSD measurement, the performances for the proposed disdrometer and PARSIVEL² are presented in Fig. 5(a) and (b) respectively. To fairly compare the measurement of these two instruments, the data from the proposed disdrometer were sorted into the same format. Concerning the RSD shapes, the proposed disdrometer exhibited almost identical results with those obtained from PARSIVEL² for the overall rainfall measurements. An empirical relationship between terminal fall velocity and raindrop diameter presented by Atlas et al. in 1973 is shown with a red curve [33]. Compared to the PARSIVEL², the proposed disdrometer measured more small raindrops (D < 0.3 mm) and large raindrops (D > 2.5 mm), but fewer moderate-size raindrops (0.3 mm < D < 2.5 mm). This observation may be owing to the higher resolution and frame rate that are beneficial to the measurement. Distinct differences are shown in the RSD of small raindrops that might be caused by the collision, coalescence, and breakup of a raindrop. The concentrated RSD shape by the PARSIVEL² is referred to as a sophisticated calibration procedure [30]. By contrast, the measurements by the proposed disdrometer provide information that is more complete. Nevertheless, a significant observation that slower falling velocities for raindrop sizes larger than 1.5 mm of the equivalent diameter [31]. The specific objective of the comparison experiment is to highlight the capability of the proposed disdrometer to facilitate the monitoring of falling raindrop dynamics through the acquisition of sequential raindrop images.

D. Evaluation of rainfall distribution of the raindrop size

To analyze the rainfall effect on raindrop sizes, the rainfall

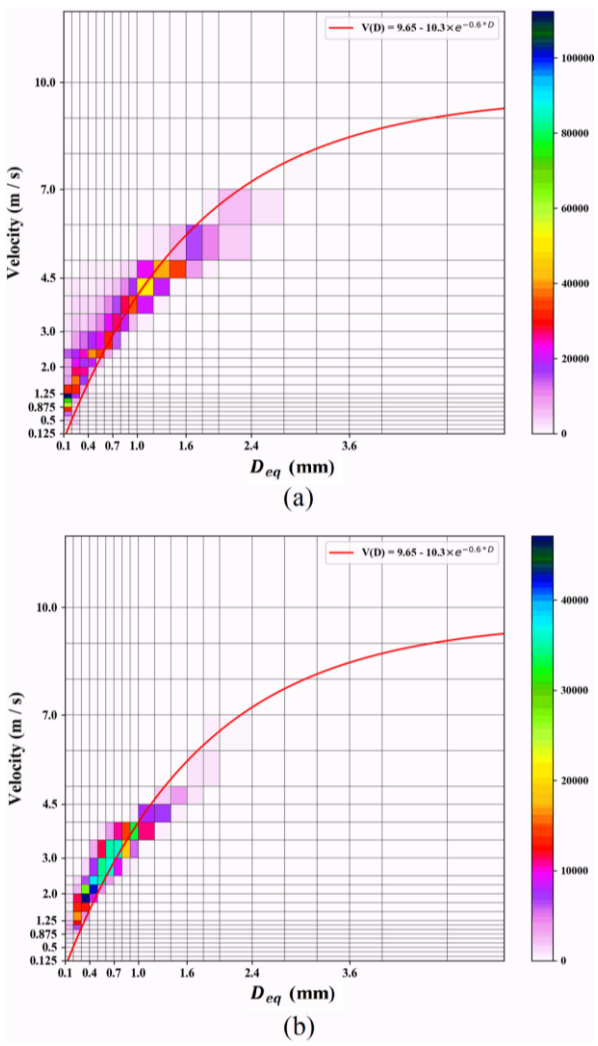

Fig. 5. Comparison of RSD measurements by (a) the proposed disdrometer, and (b) PARSIVEL² disdrometer.

ratio to raindrop size is calculated [28]. The rainfall data are classified into three groups: high rainfall, medium rainfall and low rainfall. As shown in Table III, we selected the 12th, 13th, 16th hour as high rainfall, the 2nd, 5th, 6th hours as medium rainfall, and the 1st, 4th, 7th hour as low rainfall. The corresponding average rainfall rates are 9.37 mm/h, 4.79 mm/h, and 1.73 mm/h. In Fig. 6, the rainfall ratio based on raindrop size for each group is shown. The results indicate that the primary contribution of the rainfall is medium rainfall and high rainfall with the raindrop size of 1 mm to 3 mm; this implies that small raindrops contribute little to rainfall. This finding considerably differs from the low rainfall case that concentrates on the raindrop size from 0.7 mm to 2 mm. Evidence also suggests that the rainfall rate depends primarily on both the

TABLE III
Three categories of rainfall rate versus the time interval of rainfall observations

	Rainfall Observations (Hour)	Average Rainfall Rate
High rainfall	12th, 13th, 16th	9.73 mm/h
Medium rainfall	2th, 5th, 6th	4.97 mm/h
Low rainfall	1st, 4th, 7th	1.73 mm/h

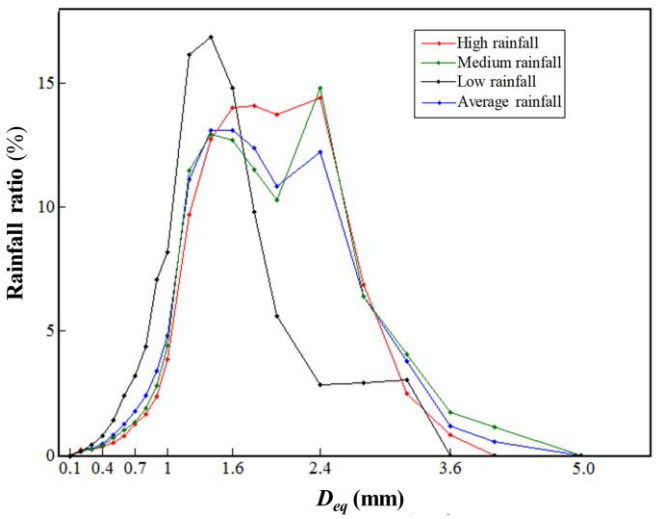

Fig. 6. Rainfall rate contribution from different raindrop size.

raindrop sizes and the associated raindrop numbers [29].

V. Conclusions

In this study, we reported a video-based disdrometer system with improved ANN technology that provided a promising and automatic approach to measure precipitation. The designed optomechanic system was used to acquire high-speed images for falling raindrops. A long depth lens was employed to address the narrow depth of focus. To adjust for the effects from a long exposure, we presented a pixel correction factor to modify the shape distortion of each raindrop. Therefore, the measurement of the raindrop size was ensured. The proposed scheme of the raindrop detection was used to segment all raindrops, and the trajectory identification algorithm was employed to determine the trajectory for each raindrop sequentially. Benefiting from the ANN classification, the proposed video-based disdrometer could achieve particle tracking with high accuracy for most raindrops. Thus, the characteristics of rainfall rate and the RSD could be computed simultaneously.

A comparison of various instruments was presented to address the differences in measurement uncertainty and facilitate in understanding the application limits. Within 42-h continuous rainfall observation, a collocated PARSIVEL^2 and a tipping-bucket rain gauge were employed in the comparison with the developed system. For the observation of the accumulated rainfall rate, the proposed system, the PARSIVEL^2 disdrometer, and a rain gauge exhibited a closer trend with only a slight variation. According to the estimates by Raupach et al., the result indicated that PARSIVEL^2 was prone to underestimating the moderate-size raindrops [30,34], which was also confirmed in our experiment. The RSD distribution measured from the proposed system agreed well with the PARSIVEL^2 disdrometer. In the analysis of the rainfall effect on different raindrop sizes, we found that the rainfall rate was dominated by both the number and size of raindrops.

Theoretically, the basic mechanism of PARSIVEL^2 is utilizing a light sheet to sense a passing raindrop; additionally, it may be susceptible to wind or heavy rain rate. Consequently, it can cause the erroneous sensing of raindrop shape and ignore the wind interference while multiple raindrops pass through the light sheets simultaneously. As for the 2DVD, it utilized two parallel light sheets in different heights that could yield errors in raindrop shapes and velocities [12]. Instead, our proposed disdrometer system was based on the acquisition of sequential frames; therefore, the rainfall information including the rainfall rate, RSD, and the associated characteristics could be obtained more precisely by evaluating the continuous movements of the raindrops. Some potential errors were eliminated effectively. Additionally, a side benefit of this approach was that the continuous process of the falling raindrops was observed in the study, which provided a comprehensive analysis of raindrop behavior.

Furthermore, the performance proved that the proposed disdrometer with low cost and low power consumption could achieve the precipitation measurement of commercial products, despite the good agreement among these three instruments that could not to fully guarantee the efficacy of the proposed disdrometer for different rain intensities and precipitation types. It is noteworthy that the purpose of this study is to construct a disdrometer of affordability, easy installation and maintenance, and hardware robustness, such that it can be applied in many applications of earth sciences, atmospheric sciences, and beyond. Therefore, more observations with long-term experiments are expected to evaluate the performances of the proposed disdrometer.

Appendix A

In this appendix, we provide an overview processes of the raindrop detection and trajectory identification to explain the details.

A. Raindrop detection

Owing to the noises and nonuniform illumination that arises from a surface light source, the raw images require preprocessing before they are employed. Therefore, a background image can be estimated by accumulating and averaging 500 frames to obtain the background reference that provides the modification of unreasonable data. A median filter with a 3×3 mask is utilized to depress speckle noises. Subsequently, Renyi entropy thresholding is used to segment the raindrops. The concept of Renyi entropy thresholding is to

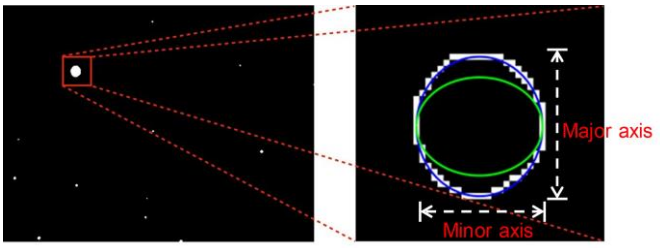

Fig. 7. Modification of the major axis of a raindrop by the pixel correction factor.

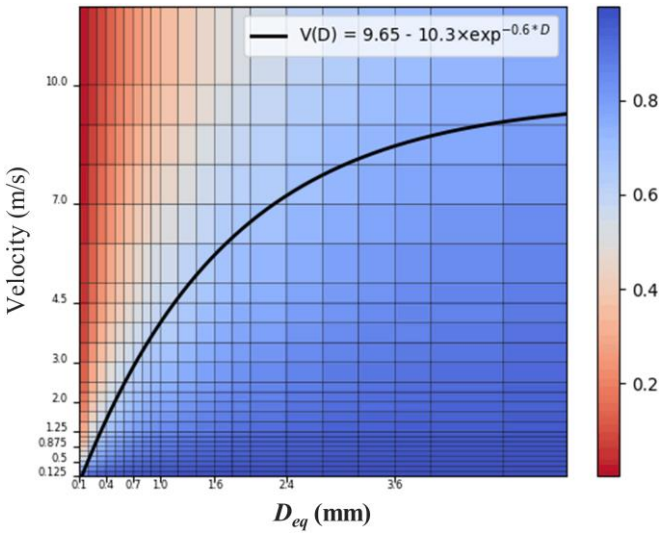

Fig. 8. Two-dimensional distribution of the pixel correction factor.

maximize two gray-level distributions of the desired raindrops.

The segmented raindrops deform distinctly while the raindrops are falling on the ground. Because of the image acquired with an exposure time, the recorded images exhibit the raindrops with distortion patterns [30]. Thus, a distortion that is corrected prior to any further processing should be applied. The detected raindrops with the corresponding velocities are used to generate the distribution of the pixel correction factor. In Fig. 7, a raindrop is shown as an example; the original and corrected shapes are superimposed, which distinctly displays a reasonable raindrop shape. Fig. 8 shows the two-dimensional distribution of the pixel correction factors according to the raindrop size, i.e. D_{eq}. The black curve is the theoretical curve of the terminal velocity of a raindrop, where the vertical axis represents the raindrop velocity, the horizontal axis represents the corresponding raindrop size, and the colors represent the various extents of the calibrating factors. The small size of a raindrop with a relatively high velocity should be modified, i.e. its major axis should be multiplied by a relatively low factor.

To ensure the accuracy of the proposed raindrop detection algorithm, the well-known sizes of the glass balls are utilized for the validation. All tests, including the raindrop size, consist of glass balls ranging from 1 mm to 5 mm, thus indicating that the errors are less than 5%.

B. Trajectory identification

Object tracking is important in many computer applications, such as object-based video compression, surveillance, and augmented reality. The following task is to obtain the probable trajectory of the same particle in any two successive frames. To avoid the situation where some trajectories may be linked to error raindrops in the previous and subsequent frames, a trajectory identification algorithm based on an ANN classification is employed. Thus, the possible trajectories of each raindrop in any two consecutive frames are through the linking estimation and subsequently searching for the most likely trajectory through the probability measures in our analysis.

The detailed procedures are summarized as follows. Let p_i and p_j denote the locations of a raindrop appearing in the 1st frame (f_1) and 2nd frame (f_2), respectively. According to the principle of terminal velocity, a raindrop and its possible candidate must be apart within a displacement, D_{ij}. The distant relation, d_{ij}, for a raindrop in any two sequences is subjected to the following condition [35,36]:

$$\left|d_{ij}\right| = \left|p_j - p_i\right| < \left|D_{ij}\right| + \left|R_j\right| \quad (4)$$

$$D_{ij} = v_{T_{ij}} \Delta t \quad (5)$$

where $v_{T_{ij}}$ is the estimated raindrop velocity according to the average size of the selected raindrop in f_1 and its possible candidate in f_2, and Δt is the duration time. R_j is the radius of the modified relaxation area in frame f_2, and centered on the position of raindrop p_j. The relaxation area implies the searching tolerance of the expected location and can be determined using differential raindrop sizes. In our case, R_j is typically affected by the wind effect and measurement errors. In the following, some features are extracted for the similarity calculation for all candidates.

1) Feature extraction

Considering the raindrops that falls to the ground surface, the motion process is dominated by the gravitational force and drag force. The majority of raindrops will be in equilibrium conditions at the terminal velocities. Based on our observation of the falling raindrops, the pattern, moving speed, and even direction of the raindrops remain unchanged within a short duration. Therefore, some valuable features of the falling raindrops can be extracted for the identification. To simplify the calculation, a minimum bounding box, e.g., an enclosing ellipse, was used to match the detected raindrop. The ellipse that was fitted to the raindrop was represented by deriving their coordinates, area, canting angle, and major and minor axes. All six features were selected as input features to feed into the trajectory identification algorithm.

2) ANN classification

The primary objective of this idea is to apply the potential of the ANN classification for the same raindrop to identify the trajectory in any successive frames. The architecture of the ANN classification with back-propagation, consisting of an input layer, four hidden layers, and an output layer, is applied. Each of the 4 hidden layers has 32, 64, 64 and 32 neurons with a rectified linear unit (ReLU) activation function and a batch normalization layer [37]. The last layer is responsible for producing the output prediction of the network. Here, we used a batch size of 32 in all our computations. The whole network was trained using the Adam optimizer [38]. To prevent overfitting, a dropout and L2 regularizer were added to each hidden layer.

Each processing element can be independently operated in parallel to add all weighted inputs and import the activation function. A general processing element can be formulated as follows:

$$y(x) = f\left(\sum_{k=1}^{n} w_i x_i\right) \tag{6}$$

where x is a neuron with n inputs$(x_1, \dots, x_n)$, out $y(x)$ and n link weights $(w_1, \dots, w_n)$ that determines the amount of gain or attenuation to be imposed to a particular input. In the output layer, f is the only selected sgmoid function,which is defined as follows:

$$f(x) = \frac{1}{1 + e^{-s(x+a)}} \tag{7}$$

where s is the steepness factor of the curve and a is a value that causes a shift away from 0. This type of sigmoid function allows the output of the neuron to change continuously. For this application, the activation is chosen to present the linking reliability of the raindrop trajectory from 0 to 1.

When performing an ANN classification, a cost value will be associated with the execution. Subsequently, each raindrop is linked to more than one trajectory, and the trajectory identification algorithm is introduced to determine the best suitable pair of raindrops from two successive frames.

3) Intersection layer

The probability of the trajectory for each raindrop is determined by performing the ANN classification. However, unexpected errors for trajectory identification may occur and therefore the iterative evaluation is beneficial for verifing the trajectory of the raindrop between any two successive frames. The intersection layer (IL) is an intuitive computation to allow all possible trajectories into the conversation. Assume four and five raindrops in the previous and subsequent frames, respectively, which indicate 20 possible probabilities. We can introduce an IL to constitute all probabilities with a vertical axis of four raindrops and a horizontal axis of five raindrops as shown in Fig. 9. Forward and backward probability measures were expressed in Figs. 9(a) and 9(b), respectively. In Fig.9 (b), another situation of the backward probability measure might be that the 4th raindrop in the previous frame is assigned to two possible raindrops, which is unlikely to occur in the real case. Therefore, the unlinked raindrops in the subsequent frame are considered to select the highest probability as the paired raindrop, i.e., the raindrop that has the largest probability. Each element in the matrix has an output probability that is labeled by using different colors, and only the highest value is chosen as a matching trajectory. Applying the computation process, each raindrop can be identified as the correct trajectory.

APPENDIX B

As the acquired raindrops can be distored, a raindrop modification procedure is suggested to solve the effect of time exposure. The following is the calculation procedure that lists each executive step.

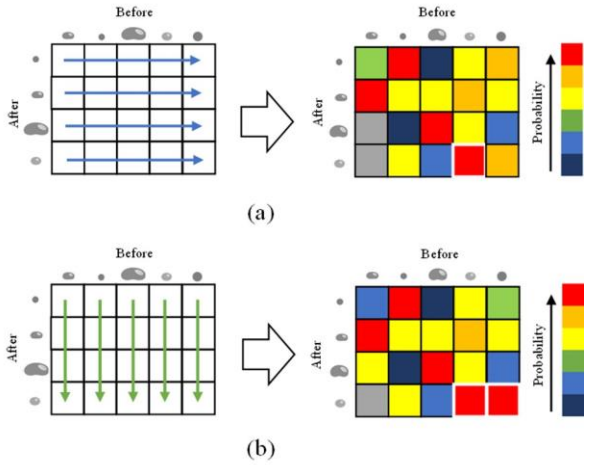

Fig. 9. Intersection layer (IL) with (a) a forward probability measure and (b) a backward probability measure for ensuring the best matching trajectory.

Raindrop Modification Algorithm

input: Velocity v; Minor axis s; Major axis l
local parameter: Calibrated major axis l';
Equivalent diameter D_{eq}
fix parameter: Exposure time t

function Calibrate rainfall (v, s, l):
$l' \longleftarrow l - v \times t$
$D_{eq} \longleftarrow (s \times l'^2)^{\frac{1}{3}}$
$V \longleftarrow \pi/6 \times (s \times l'^2)$
return Equivalent diameter D_{eq};
Calibrated raindrop volume V

REFERENCES

[1] C. Prigent, "Precipitation retrieval from space: An overview," *Comptes. Rendus. Geoscience*., vol. 342, no. 4-5, pp. 380–389, Apr. 2010.
[2] B. Chapon, G. Delrieu, M. Gosset, and B. Boudevillain, "Variability of rain drop size distribution and its effect on the Z–R relationship: A case study for intense Mediterranean rainfall," *Atmos. Res.*, vol. 87, no. 1, pp. 52–65, Jan. 2008.
[3] A. B. Kostinski and R. A. Shaw, "Droplet dynamics: Raindrops large and small," *Nat. Phys.*, vol. 5, no. 9, pp. 624–625, Sep. 2009.
[4] S. Das and A. Maitra, "Characterization of tropical precipitation using drop size distribution and rain rate-radar reflectivity relation," *Theor. Appl. Climatol*., vol. 132, no. 1-2, pp. 275–286, 2018,
[5] G. Vulpiani, F. S. Marzano, V. Chandrasekar, A. Berne and R. Uijlenhoet, "Polarimetric weather radar retrieval of raindrop size distribution by means of a regularized artificial neural network,". *IEEE Trans. Geosci. Remote Sens.*, vol. 44, no. 11, pp. 3262–3275, *Nov*. 2006.
[6] R. Onishi, K. Matsuda and K. Takahashi, "Lagrangian tracking simulation of droplet growth in turbulence–turbulence enhancement of autoconversion rate," J. Atmos. Sci., vol. 72, no. 7, pp. 2591–2607, Jul. 2015.
[7] J. R. Valentine and R. A. Decker, "A Lagrangian-Eulerian scheme for flow around an airfoil in rain. Int. J. Multiphas Flow, vol. 21, no. 4, pp. 639–648, Aug. 1995.
[8] G. Kathiravelu, T. Lucke and P. Nichols, "Rain drop measurement techniques: a review," *Water*, vol. 8, no. 1, pp. 29, Jan. 2016.

[9] J. Jaffrain and A. Berne, "Experimental quantification of the sampling uncertainty associated with measurements from PARSIVEL disdrometers," *J. Hydrometeorol.*, vol. 12, no. 3, pp. 352–370, 2011.
[10] M. Löffler-Mang, and J. Joss, "An optical disdrometer for measuring size and velocity of hydrometeors," *J. Atmospheric Ocean. Technol.*, vol. 17, no. 2, pp. 130–139, Feb. 2000.
[11] M. Schönhuber, G. Lammer and W. L. Randeu, "One decade of imaging precipitation measurement by 2D-video-disdrometer," *Adv. Geosci.*, vol. 10, pp. 85–90, Apr. 2007.
[12] H. Leijnse and R. Uijlenhoet, "The effect of reported high-velocity small raindrops on inferred drop size distributions and derived power laws," *Atmos. Chem. Phys.*, vol. 10, no. 14, pp. 6807-6818, Jul. 2010.
[13] Testik, F. Y. and M. K. Rahman. "High-speed optical disdrometer for rainfall microphysical observations," *J. Atmospheric Ocean. Technol.*, vol. 33, no. 2, pp. 231–243, Feb. 2016.
[14] J. R. Saylor and N. A. Sivasubramanian, "Edge detection methods applied to the analysis of spherical raindrop images," *Appl. Optics*, vol. 46, pp. 5352–5367, 2007.
[15] M. Raffel, C. E. Willert, S.T. Wereley, J. Kompenhans, "Particle image velocimetry : a practical guide," Experimental fluid mechanics. Springer, Berlin, New York, 2007.
[16] H. C. Yang and F. J.Chang "Modelling combined open channel flow by artificial neural network," *Hydrol. Process.*, 19, pp. 3747–3762, Aug. 2005.
[17] A. Yilmaz, O. Javed and M. Shah, "Object tracking: A survey," Acm computing surveys (CSUR), vol. 38, no. 4, pp. 13, 2006.
[18] D. Comaniciu, V. Ramesh, and P. Meer, "Real-time tracking of non-rigid objects using mean shift," IEEE Conf. on Comp. Vis. and Pat. Rec., Hilton Head Island, South Carolina, 2000.
[19] H. Zhou and G. Schaefer, "Non-rigid object tracking," In ELMAR, PROCEEDINGS IEEE, pp. 101–104, Sep. 2010.
[20] Y. A. Hassan and O. G. Philip. "A new artificial neural network tracking technique for particle image velocimetry," *Exp. Fluids*, vol. 23, no. 2, pp. 145–154, 1997.
[21] T. A. Dolenko, S. A. Burikov, A. M. Vervald, I. I. Vlasov, S. A. Dolenko, K. A. Laptinskiy, J. M. Rosenholm and O. A. Shenderova, "Optical imaging of fluorescent carbon biomarkers using artificial neural networks," *J. Biomed Opt.*, vol. 19, no. 11, pp. 117007, Jan. 2014.
[22] Y. Ge, S. S. Cha and J. H. Park, "Study of particle tracking algorithms based on neural networks for stereoscopic tracking velocimetry," *Opt. Laser Eng.*, vol. 44, no. 6, pp. 623–636, Jun. 2006.
[23] Rabault, Jean, Jostein Kolaas, and Atle Jensen, "Performing particle image velocimetry using artificial neural networks: a proof-of-concept," *Meas. Sci. Technol.*, vol. 28, no.12, pp. 125301, Nov. 2017.
[24] D. E. Rumelhart, G. E. Hinton and R. J. Williams, "Learning representations by backpropagating errors," *Nature*, vol. 323, no. 9, pp. 533–536, 1986.
[25] J. N. Kutz, "Deep learning in fluid dynamics," *J. Fluid Mech.*, vol. 814, pp. 1–4, Jan. 2017.
[26] J. Rabault, M. Kuchta, A. Jensen, U. Réglade and N. Cerardi, "Artificial neural networks trained through deep reinforcement learning discover control strategies for active flow control," *J. Fluid Mech.*, vol. 865, pp. 281–302. 2019.
[27] D. Valero and D. B. Bung, "Artificial Neural Networks and pattern recognition for air-water flow velocity estimation using a single-tip optical fibre probe," *J. Hydro-Environ Res.*, vol. 19, pp.150–159, Mar. 2018.
[28] M. Godec, P. M. Roth and H. Bischof, "Hough-based tracking of non-rigid objects," *Comput. Vis. Image Und.*, vol. 117, no. 10, pp. 1245–1256, Oct. 2013.
[29] L. A. Zarrabeitia, F. Z. Qureshi and D. A. Aruliah, "Stereo reconstruction of droplet flight trajectories," *IEEE Trans. Pattern Anal. Mach. Intell.*, vol. 37, no. 4, pp. 847–861, Apr. 2015.
[30] T. H. Raupach and A. Berne, "Correction of raindrop size distributions measured by Parsivel disdrometers, using a two-dimensional video disdrometer as a reference," *Atmos. Meas. Tech.*, vol. 8, no. 1, pp. 343–365, 2015.
[31] A. Tokay, W. A. Petersen, P. Gatlin and M. Wingo, "Comparison of raindrop size distribution measurements by collocated disdrometers," *J. Atmospheric Ocean. Technol.*, vol. 30, no. 8, pp. 1672–1690, Aug. 2013.
[32] P. Sahoo, C. Wilkins and J. Yeager, "Threshold selection using Renyi's entropy," *Pattern Recognit.*, vol. 30, no. 1, pp. 71–84, Jan. 1997.
[33] K. Ohmi and H. Y. Li, "Particle-tracking velocimetry with new algorithms," *Meas. Sci. Technol.*, vol. 11, no. 6, pp. 603–616. (2000).
[34] S. G. Park, H. L., Kim, Y. W. Ham and S. H. Jung, "Comparative evaluation of the OTT PARSIVEL^2 using a collocated two-dimensional video disdrometer," *J. Atmospheric Ocean. Technol.*, vol. 34, no. 9, pp. 2059-2082. Sep. 2017.
[35] F. Pereira, H. Stüer, E. C. Graff and M. Gharib, "Two-frame 3D particle tracking," *Meas. Sci. Technol.*, vol. 17, no. 7, pp. 1680–1692, Jun. 2006.
[36] L. Shindler, M. Moroni and A. Cenedese, "Spatial–temporal improvements of a two-frame particle-tracking algorithm," *Meas. Sci. Technol.*, vol. 21, no. 11, pp. 115401, Nov. 2010.
[37] A. Radford, L. Metz and S. Chintala, "Unsupervised representation learning with deep convolutional generative adversarial networks," arXiv preprint arXiv:1511.06434, 2015.
[38] D. Kingma and J. Ba. "Adam: A method for stochastic optimization,". In: arXiv preprint arXiv:1412.6980, 2014.

Chi-Wen Hsieh received the B.Sc. in Department of Physics from Fu-Jen Catholic University, Taiwan, ROC in 1990. And he received Master and Ph.D. degrees in Department of Electrical Engineering from National Tsing-Hua University, Taiwan, ROC in 1993 and 2007. Now he is chair and professor for the Department of Electrical Engineering of National Chiayi University, Taiwan, ROC since 2018. Currently, his research interests include medical signal processing, microwave applications, and image processing.

Po-Wei Chi was born in Tainan, Taiwan, in 1995. He received his Bachelor degree in electrical engineering, National Chiayi University, Taiwan. Currently, he is pursuing his master's degree in electrical and computer engineering, University of California, Davis. His research interests include in image processing and machine learning.

Chih-Yen Chen (M'10–SM'18) received the master's degree in physics from National Taiwan Normal University, Taiwan, in 2003, and Ph.D. degree in Biomedical Engineering from National Yang-Ming University in 2010, Taiwan. Currently, he is an assistant researcher with Instrument Technology Research Center, National Applied Research Laboratories (NARLabs), Taiwan. He is an IEEE member and IEEE Instrument and Measurement Society member. His research interests include instrument development for pattern recognition, disaster instrument and optical measurement.

Chun-Jen Weng (M'15) received his Ph.D. in electro-optical engineering from National Chiao Tung University. He is currently a research fellow & team leader of optical instrument at the Taiwan Instrument Research Institute, National Applied Research Laboratories. His research interests are in the area of microspectrophotometry, hyperspectral imaging and tunable confocal laser system. Dr. Weng is a member of IEEE and a member of the Optical Society of America (OSA) and the International Society for Optics and Photonics (SPIE).

Lijuan Wang (M'14) received the B.Eng. degree in computer science and technology from Qiqihar University, Heilongjiang Province, China, in 2010, and the Ph.D. degree in measurement and automation from North China Electric Power University, Beijing, China, in 2015 and the Ph.D. degree in electronic engineering from the University of Kent, Canterbury, UK, in 2017. She is currently a Lecturer in Electronic Engineering with the School of Engineering and Digital Arts, University of Kent. Her current research interests include electrostatic sensing, multiphase flow measurement, condition monitoring of mechanical systems, sensors and instrumentation systems data analysis and soft computing.